



HAL
open science

Comparative immune profiling of acute respiratory distress syndrome patients with or without SARS-CoV2 infection

Mikaël Roussel, J. Ferrant, F. Reizine, S. Le Gallou, J. Dulong, S. Carl, M. Lesouhaitier, M. Gregoire, N. Bescher, C. Verdy, et al.

► To cite this version:

Mikaël Roussel, J. Ferrant, F. Reizine, S. Le Gallou, J. Dulong, et al.. Comparative immune profiling of acute respiratory distress syndrome patients with or without SARS-CoV2 infection. *Cell Reports Medicine*, 2021, 2 (6), pp.100291. 10.1016/j.xcrm.2021.100291 . hal-03229515

HAL Id: hal-03229515

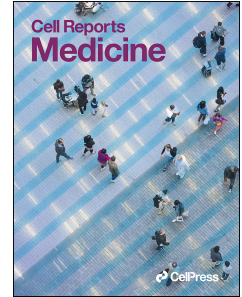
<https://hal.sorbonne-universite.fr/hal-03229515>

Submitted on 19 May 2021

HAL is a multi-disciplinary open access archive for the deposit and dissemination of scientific research documents, whether they are published or not. The documents may come from teaching and research institutions in France or abroad, or from public or private research centers.

L'archive ouverte pluridisciplinaire **HAL**, est destinée au dépôt et à la diffusion de documents scientifiques de niveau recherche, publiés ou non, émanant des établissements d'enseignement et de recherche français ou étrangers, des laboratoires publics ou privés.

Journal Pre-proof



Comparative immune profiling of acute respiratory distress syndrome patients with or without SARS-CoV2 infection

M. Roussel, J. Ferrant, F. Reizine, S. Le Gallou, J. Dulong, S. Carl, M. Lesouhaitier, M. Gregoire, N. Bescher, C. Verdy, M. Latour, I. Bézier, M. Cornic, A. Vinit, C. Monvoisin, B. Sawitzki, S. Leonard, S. Paul, J. Feuillard, R. Jeannet, T. Daix, V.K. Tiwari, J.M. Tadié, M. Cogné, K. Tarte

PII: S2666-3791(21)00119-1

DOI: <https://doi.org/10.1016/j.xcrm.2021.100291>

Reference: XCRM 100291

To appear in: *Cell Reports Medicine*

Received Date: 3 December 2020

Revised Date: 14 March 2021

Accepted Date: 29 April 2021

Please cite this article as: Roussel, M., Ferrant, J., Reizine, F., Le Gallou, S., Dulong, J., Carl, S., Lesouhaitier, M., Gregoire, M., Bescher, N., Verdy, C., Latour, M., Bézier, I., Cornic, M., Vinit, A., Monvoisin, C., Sawitzki, B., Leonard, S., Paul, S., Feuillard, J., Jeannet, R., Daix, T., Tiwari, V.K., Tadié, J.M., Cogné, M., Tarte, K., Comparative immune profiling of acute respiratory distress syndrome patients with or without SARS-CoV2 infection, *Cell Reports Medicine* (2021), doi: <https://doi.org/10.1016/j.xcrm.2021.100291>.

This is a PDF file of an article that has undergone enhancements after acceptance, such as the addition of a cover page and metadata, and formatting for readability, but it is not yet the definitive version of record. This version will undergo additional copyediting, typesetting and review before it is published in its final form, but we are providing this version to give early visibility of the article. Please note that, during the production process, errors may be discovered which could affect the content, and all legal disclaimers that apply to the journal pertain.

© 2021

Patients in ICU

COVID-19^{pos} ARDS^{pos}
 COVID-19^{neg} ARDS^{pos}
 COVID-19^{pos} ARDS^{neg}

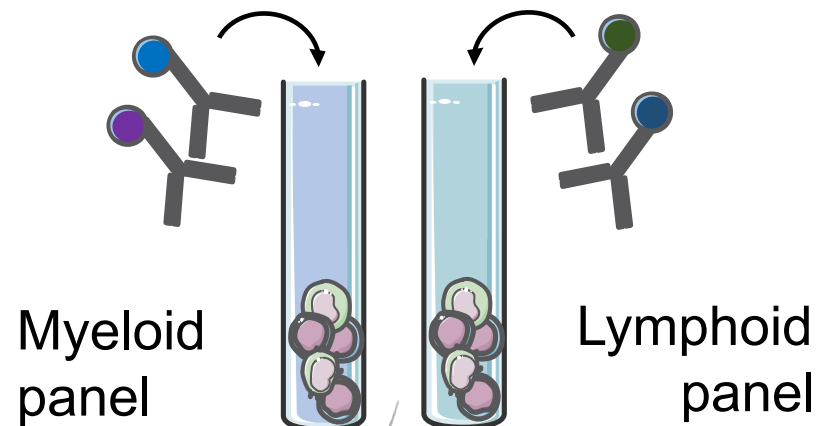
Cohort 1

Cohort 2

D0 D7
 ───────────────────▶

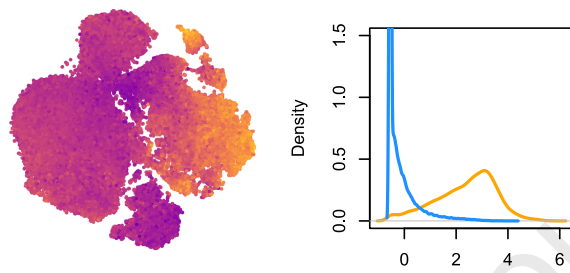


Mass Cytometry



Machine-learning based algorithm

CellCnn



Algorithm guided analysis

viSNE, FlowSOM



Covid-19 signature

CD169^{pos} S100A9^{pos}
 activated monocytes

Th1-like
 effector T cells

Plasmablasts &
 Plasma cells

Adverse clinical evolution markers

CD14^{pos} HLA-DR^{lo}
 M-MDSC-like cells

CD14^{lo} CD16^{pos}
 non-classical monocytes

First days in ICU

Comparative immune profiling of acute respiratory distress syndrome patients with or without SARS-CoV2 infection

M. Roussel^{1,2,3,16,17*}, J. Ferrant^{3,16}, F. Reizine^{3,4}, S. Le Gallou^{2,3}, J. Dulong^{2,3}, S. Carl⁵, M. Lesouhaitier^{3,4}, M. Gregoire^{2,3}, N. Bescher², C. Verdy², M. Latour², I. Bézier², M. Cornic², A. Vinit⁶, C. Monvoisin³, B. Sawitzki⁷, S. Leonard¹, S. Paul⁸, J. Feuillard⁹, R. Jeannet^{9,10,11}, T. Daix^{11,12,13}, V.K. Tiwari^{5,14}, J.M. Tadié^{3,4}, M. Cogné^{3,15,16}, K. Tarte^{2,3,16*}

¹Centre Hospitalier Universitaire de Rennes, Laboratoire Hématologie, Pôle Biologie, F-35033, Rennes, France

²Centre Hospitalier Universitaire de Rennes, SITI, Pôle Biologie, F-35033, Rennes, France

³Institut national de la santé et de la recherche médicale, Unité Mixte de Recherche U1236, LabEx IGO, Université Rennes 1, Etablissement Français du Sang Bretagne, F-35000, Rennes, France

⁴Centre Hospitalier Universitaire de Rennes, Maladies Infectieuses et Réanimation Médicale, F-35033, Rennes, France

⁵Scailyte AG, CH-6210, Sursee, Switzerland

⁶Sorbonne Université, UMS037, PASS, Plateforme de Cytométrie de la Pitié-Salpêtrière CyPS, F-75013, Paris, France

⁷Charité - Universitätsmedizin Berlin, Institut für Medizinische Immunologie, AG Molekulare Immunmodulation, D-13353, Berlin, Germany

⁸Centre Hospitalier Universitaire de Saint-Etienne, Laboratoire Immunologie, F-42000, Saint-Etienne, France

⁹Centre Hospitalier Universitaire de Limoges, Laboratoire Hématologie, F-87000, Limoges, France

¹⁰Unité Mixte de Recherche CNRS 7276 INSERM 1262, F-87000, Limoges, France

¹¹Centre d'investigation Clinique INSERM 1435, F-87000, Limoges, France

¹²Unité Mixte de Recherche INSERM 1092, F-87000, Limoges, France

¹³Centre Hospitalier Universitaire de Limoges, Service de Réanimation Médicale, F-87000, Limoges, France

¹⁴Wellcome-Wolfson Institute for Experimental Medicine, School of Medicine, Dentistry & Biomedical Science, Queens University Belfast, BT9 7BL, United Kingdom

¹⁵Centre Hospitalier Universitaire de Rennes, Laboratoire Immunologie, Pôle Biologie, F-35033, Rennes, France

¹⁶ These authors contributed equally

¹⁷Lead contact

*Correspondence to: mikael.roussel@chu-rennes.fr (M.R.); karin.tarte@univ-rennes1.fr (K.T.)

Summary

Acute respiratory distress syndrome (ARDS) is the main complication of COVID-19, requiring admission to Intensive Care Unit (ICU). Despite extensive immune profiling of COVID-19 patients, to what extent COVID-19-associated ARDS differs from other causes of ARDS remains unknown. To address this question, we build 3 cohorts of patients categorized in COVID-19^{neg}ARDS^{pos}, COVID-19^{pos}ARDS^{pos}, and COVID-19^{pos}ARDS^{neg}, and compare their immune landscape analyzed by high-dimensional mass cytometry on peripheral blood. A cell signature associating S100A9/calprotectin-producing CD169^{pos} monocytes, plasmablasts, and Th1 cells is found in COVID-19^{pos}ARDS^{pos}, unlike COVID-19^{neg}ARDS^{pos} patients. Moreover, this signature is essentially shared with COVID-19^{pos}ARDS^{neg} patients, suggesting that severe COVID-19 patients, whatever they experience or not ARDS, display similar immune profiles. We show an increase in CD14^{pos}HLA-DR^{low} and CD14^{low}CD16^{pos} monocytes correlate to the occurrence of adverse events during ICU stay. We demonstrate that COVID-19-associated ARDS display a specific immune profile, and might benefit from personalized therapy in addition to standard ARDS management.

Introduction

The SARS-Coronavirus-2 (SARS-CoV-2) virus has rapidly affected more than 30 million people worldwide, requiring admission to Intensive Care Unit (ICU) for more than 2 million patients.¹ Whereas most patients exhibit mild-to-moderate symptoms, acute respiratory distress syndrome (ARDS) is the major complication of the coronavirus disease 2019 (COVID-19),^{2,3} leading to prolonged ICU stays, and high frequency of secondary complications, notably cardiovascular events, thrombosis, pulmonary embolisms, and strokes.^{1,4} The immune system plays a dual role in COVID-19, contributing to both virus elimination and ARDS development.⁵ Excessive inflammatory response has been proposed as the leading cause of COVID-19-related clinical complications, thus supporting intensive efforts to better understand the specificities and mechanisms of SARS-CoV-2-induced immune dysfunction.^{6,7} Moreover, even if therapies such as provided by convalescent plasma or neutralizing antibodies at an early stage of the disease, can lower the viral burden, this was only demonstrated in specific populations such as aged patients over 75,⁸ and no antiviral treatment has yet been able to definitely prevent the evolution of some patients towards deregulated inflammation and critical respiratory complications. The benefit of corticosteroids in severe COVID-19 for lowering overall mortality is now widely acknowledged.^{9,10} Conversely, steroid therapy was shown harmful in other ARDS etiologies, such as in influenza-associated ARDS,¹¹ suggesting specific biological features of COVID-19-related ARDS. A detailed understanding of the COVID-19-specific immune dysfunctions underlying ARDS development and severity is thus a major need and will hopefully help adapt specific therapeutic strategy.

A number of high-resolution studies have recently concentrated on the determination of circulating markers that can distinguish severe from mild forms of COVID-19, providing a tremendous amount of data describing phenotypic and functional alterations in T cell, B cell, and

myeloid cell subsets.^{12–25} In particular, CD14^{pos}HLA-DR^{low}, CD14^{pos}CD16^{pos}, and immature monocytes were demonstrated as increased among peripheral blood mononuclear cells (PBMCs) from critically ill COVID-19 patients.^{15,21,23,26–29} Interestingly, monocyte number is reduced in COVID-19 compared to influenza patients, suggesting specific myeloid dysregulation.³⁰ Various COVID-19-related alterations of lymphoid cells have also been described, including a T-cell lymphopenia, predictive of patient outcome, a broad T-cell activation including Th1, Th2, and Th17, an alteration of B-cell and T-cell repertoires, and a strong increase of plasmablasts, most prominent in ARDS COVID-19 patients.^{14,17,25,31–33} Importantly, COVID-19 ARDS immune profiling was performed using healthy donors as a control, thus precluding any conclusions on whether reported immune alterations could be related to COVID-19 and/or ARDS status. Answering this question has potential to decipher whether ARDS induced by SARS-CoV-2 is mechanistically different from other ARDS etiologies.

To fill this gap, we performed a high-throughput mass cytometry approach on PBMCs obtained from 3 complementary series of 18 COVID-19^{neg}ARDS^{pos}, 18 COVID-19^{pos}ARDS^{pos}, and 20 COVID-19^{pos}ARDS^{neg} patients, including exploratory and validation cohorts. We report common myeloid cell alterations in all COVID-19 patients, which are absent from non-COVID-19 ARDS patients. This includes in particular a strong increase of an unusual population of activated monocytes showing upregulated expression of CD169, associated with major COVID-19-specific alterations of T and B-cell compartments.

Results

Study population

Analyses were performed on a cohort of 63 cryopreserved PBMC samples isolated from 42 patients included in ICU (n = 36) or infectious standard ward (n = 6). The demographic

characteristics of patients included are provided in Table 1 and Table S1. All patients but one were classified as severe at admission, requiring oxygen at a flow rate higher than 2 liters/min. ARDS was defined in accordance with international guidelines.³⁴ Patients were classified in 3 groups: COVID-19^{neg}ARDS^{pos} (n = 12, ARDS stages: 1 mild, 4 moderate, 7 severe), COVID-19^{pos}ARDS^{pos} (n = 13, ARDS stages: 8 moderate, 5 severe), and COVID-19^{pos}ARDS^{neg} (n = 17, including 11 from ICU and 6 from infectious standard ward). In the COVID-19^{pos}ARDS^{neg}, no statistical differences were noticed for immune cell abundance or phenotype between ICU and standard ward patients. Within the COVID-19^{neg}ARDS^{pos} group, ARDS etiologies were bacterial pneumonia (n = 9), anti-synthetase syndrome (n = 1), and unknown (n = 2) (Table S1). For 21 patients, a second blood sample obtained on day 7 after enrollment was studied (n = 7 for COVID-19^{neg}ARDS^{pos}, n = 8 for COVID-19^{pos}ARDS^{pos}, and n = 6 for COVID-19^{pos}ARDS^{neg}). Additionally, a validation cohort (cohort 2) was set up with 16 patients with demographic data detailed in Table S1 and Table S2. Patients were classified in 3 groups: COVID-19^{neg}ARDS^{pos} (n = 6), COVID-19^{pos}ARDS^{pos} (n = 5), and COVID-19^{pos}ARDS^{neg} (n = 3); additionally, COVID-19^{neg}ARDS^{neg} (n = 2) samples were included. None of our patients received corticosteroids at the time of the study nor immune-modulators. The presence of SARS-CoV-2 in respiratory specimens (nasal and pharyngeal swabs or sputum) was detected by real-time reverse transcription polymerase chain reaction (RT-PCR) methods. To rule out undetected infections, negative RT-PCR samples were confirmed when possible by absence of neutralizing antibodies. Neutralizing antibodies were undetectable for the 11 samples out of 18 COVID-19^{neg} patients for which material was available. In contrast, neutralizing antibodies were detected in 29 out of 30 COVID-19^{pos} tested. Timeline of sample collection are shown in Fig. S1.

SARS-CoV2 induces phenotypic changes in circulating immune cells

To decipher the impact of SARS-CoV2 on circulating immune cells, we characterized PBMCs from COVID-19^{pos} versus COVID-19^{neg} patients at admission using two separate mass cytometry panels exploring myeloid and lymphoid subsets, respectively (Table S3 and Key Resources Table). The full pipeline of analysis is depicted in Fig. S1. First, we performed an unbiased discovery approach with CellCnn, a neural network-based artificial intelligence algorithm allowing analysis of single-cell data and detection of cells associated with clinical status.³⁵⁻³⁷ During training, CellCnn learns combinations of weights for each marker in a given panel that best discriminate between groups of patients. These weight combinations, called filters, can be used to highlight the specific profiles of cells associated with patient status. We identified the best-performing CellCnn filters for both the myeloid and the lymphoid panels highlighting a population of cells significantly enriched in COVID-19^{pos} patients as compared to COVID-19^{neg} patients ($P < 0.0001$ for both panels) (Fig. 1A). Projecting these cells on tSNE maps generated with either the myeloid or the lymphoid panels revealed that they fell into several distinct areas (Fig. 1B). The cells selected by the CellCnn filter on the myeloid panel showed high expression for CD169, CD64, S100A9, CD11b, CD33, CD14, and CD36 compared to background, while the cells selected by the CellCnn filter on the lymphoid panel showed high expression for CD38 and CXCR3 (Fig.1B and Fig. S2). These results were replicated in the cohort 2 (Fig. S3), and confirmed on a public set of data by using the CellCnn analysis showing a high expression of CD14, CD36, CD64, and CD169 cells on COVID-19^{pos} patients (Fig. S4).¹⁵ As a whole, this broad and unbiased approach reproducibly showed that immune markers, in particular related to monocytes, segregated COVID-19^{neg} and COVID-19^{pos} patients.

SARS-CoV2 induces CD169-expressing monocyte subsets

To investigate circulating monocyte heterogeneity and define consistent phenotypes, we used the FlowSOM algorithm. This approach led to the identification of 15 monocyte metaclusters from the myeloid panel (Fig. 2A). In particular, Mo30, Mo11, and Mo28 metaclusters were defined by higher expression of CD16 and lower expression of CD14, CD36, and CD64, corresponding to a non-classical monocyte phenotype. Mo21 and Mo22 were defined by the high expression of S100A9 and the low expression of CD36. Finally, Mo243 and Mo180 strongly expressed S100A9, CD169, and CD36. To assess the phenotypic changes in monocytes during SARS-CoV2 infection, we determined the frequencies of these metaclusters in each patient at admission and performed hierarchical clustering on these values (Fig. 2B). The upper branch of the hierarchical clustering included 20 COVID^{pos} (10 ARDS^{neg} and 10 ARDS^{pos}) and 1 COVID^{neg}ARDS^{pos} patient whereas the lower branch included 10 COVID^{pos} (7 ARDS^{neg} and 3 ARDS^{pos}) and 11 COVID^{neg}ARDS^{pos} (chi-square = 0.001) (Fig. 2B). We then analyzed the abundance of individual metaclusters and identified only 4 metaclusters out of 15 as differentially represented between the 3 groups of patients (Fig. 2C and Fig. S2). In particular, within ARDS^{pos} patients, Mo11 and Mo181 were less abundant in COVID-19^{pos} patients ($P < 0.01$ and $P < 0.05$, respectively), while Mo243 and Mo180 were more abundant ($P < 0.05$ and $P < 0.001$) (Fig. 2C). No differences were detected within COVID-19^{pos} groups (ARDS^{pos} versus ARDS^{neg}) (Fig. 2C). Interestingly, Mo243 and Mo180 were both enriched in cells highly expressing CD169, CD64, CD36, and CD14 (Fig. 2A and 2D). Additionally, Mo22 was present only in some COVID^{pos} patients and also expressed CD169 (Fig. 2B). Taken together, Mo243, Mo180, and Mo22 metaclusters were highly enriched in COVID-19^{pos} patients when compared to COVID-19^{neg} patients ($P < 0.0001$), with no difference regarding the ARDS status (Fig. 2E). Accordingly, CD169 was differentially expressed in COVID-19^{pos} versus COVID-19^{neg} patients ($P < 0.001$) (Fig. 2E). Altogether, our study including COVID-19 and non-COVID-19 critically ill patients suggest a specificity of

CD169 expression in COVID-19 patients, and greatly extend previous scRNAseq data showing an expansion of CD169-expressing monocytes in COVID-19 patients compared to healthy donors (Fig. 2F).^{15,25,38-40} We then performed the FlowSOM analysis on cohort 2 and validated the enrichment of Mo243 and Mo180 in COVID-19^{pos} samples (Fig. S3A, S3B), these metaclusters also presenting a trend for high CD169 expression (Fig. S3C).

Monocyte metacluster enrichment in COVID-19 is correlated with a specific increase of effector memory T cells and plasma cells

To define a more global immune pattern and the relationship between immune cells in the context of the SARS-CoV2 infection, we sought for correlation between frequencies of clusters of T-, NK-, B-, and plasma cells ($n = 136$ clusters from the lymphoid panel, Fig. S1) and the 4 monocyte metaclusters (Mo11, Mo181, Mo243, and Mo180) previously described. This analysis identified 70 clusters with significantly correlated variations ($P < 0.05$) (Fig. S2). To strengthen the relevance of these correlations, we restrained further analysis to the 29 strongest relationships ($R > 0.5$ or < -0.5 and $P < 0.01$) between Mo180 or Mo243 (the two metaclusters enriched in COVID-19 patients) and other immune cell subsets (Fig. 3A and Table S4). As expected, Mo180 and Mo243 metaclusters were correlated ($R = 0.93$). Moreover, they were positively correlated with 18 clusters of T ($n = 6$), NK ($n = 10$), and plasma cells ($n = 2$), and inversely correlated with 11 clusters of T ($n = 9$), and NK cells ($n = 2$) (Fig. 3A). Among positively correlated clusters, plasm_183 and plasm_198 similarly expressed CD38, CD44, and CD27, whereas plasm_183 was high for Ki-67 and HLA-DR, corresponding to an early plasma cell phenotype (Fig. 3B). NK cells were all marked by CD7 and T-bet expression, NK_209 being CD8^{high}, and NK_241 and NK_197 displaying a Ki-67^{high} proliferating phenotype. The related T8_147 and T8_161 clusters exhibited a CD45RA^{high}CD45RO^{low}CCD7^{low}CD27^{low}Tbet^{high}CD38^{high} effector phenotype. Few

T4 clusters were positively correlated with Mo180 and Mo243, among them T4_106 displayed an effector memory proliferating phenotype (Ki-67^{high}CD45RA^{low}CCR7^{low}CD45RO^{high}CD27^{high} and CTLA4^{high}PD1^{high}). T4_25 was also marked by an effector memory phenotype (CD45RA^{low}CCR7^{low}CD45RO^{pos}) and displayed a CD27^{low}CD127^{pos}CCR6^{pos}CxCR3^{neg}CD161^{pos} Th17 profile (Fig. 3B). Conversely, some T4 clusters were inversely correlated with Mo_180 and Mo_243, in particular clusters T4_6, T4_20, and T4_34, all three corresponding to naïve cells (CD45RA^{high}CD45RO^{low}CCR7^{high}), and T4_59 expressing a Th2 phenotype (CCR4^{high}). We then compared the abundance of these 29 lymphoid clusters correlated with Mo180 and Mo243 and highlighted the 22 differentially represented lymphoid clusters between the three groups of patients ($P < 0.05$) (Fig. 3C and Fig. S2). Only 7 clusters of CD4 T cells, and 2 clusters of CD8 T cells were at lower abundance in COVID-19^{pos}ARDS^{pos} patients compared to COVID-19^{neg}ARDS^{pos} patients. As previously discussed, T4_6, T4_20, and T4_34 corresponded to naïve cells, whereas within the effector memory cells, T4_7 and T4_45 were CD127^{low}, T4_24, T8_99, and T8_113 were CD127^{high}, and T4_59 was CCR4^{high}. Conversely, 13 clusters were enriched in COVID-19^{pos}ARDS^{pos} compared to COVID-19^{neg}ARDS^{pos} including: i) CTLA4^{high}PD1^{high} effector memory activated CD4 Tcells (T4_106); ii) Tbet^{high} Th1-like CD8 effector phenotype (T8_146, T8_147, and T8_161); iii) cytotoxic mature CD16^{pos}CD56^{low}CD7^{pos}Tbet^{pos}CD127^{neg} NK cells (NK_209, NK_241, NK_242, and NK_244) with in particular proliferating Ki-67^{high} NK cells (NK_241); and iv) proliferating plasmablasts (plasma_183) and mature plasma cells (plasma_198) (Fig. 3B and Fig. 3C). Of note, no cluster was differentially expressed between COVID-19^{pos}ARDS^{pos} and COVID-19^{pos}ARDS^{neg} groups (Fig. 3C and Fig. S2). Then, to explore the whole immune profile and define relationship with groups of patients, we performed correspondence analysis (CA) using, as a variable, the abundance of the myeloid ($n = 4$) and the lymphoid ($n = 22$) clusters differentially expressed between groups of patients (Fig. 3D). CA was

developed to analyze frequency tables and visualize similarities between patients and co-occurrence of cell subsets.⁴¹ The first and second dimension of the correspondence analysis explained 80.5 % and 13.5 % of the difference, respectively (Fig. 3D). The top-ten cell populations accounting for the difference between COVID^{pos} and COVID^{neg} patients were Mo243, Mo180, T8_146, NK_244, and T8_161 being increased and Mo181, T4_6, Mo11, T8_99, and T4_45 being decreased in COVID^{pos}. Altogether, these subsets corresponded to an increase in inflammatory monocytes (CD169^{high} CD64^{high}), Tbet^{high} Th1-like CD8 T cells, and mature NK cells and a decrease in naïve T4 cells and effector memory T4 and T8 cells. Interestingly, only the first dimension of the correspondence analysis segregated COVID-19^{pos} ARDS^{pos} from COVID-19^{neg} ARDS^{pos} ($P < 0.001$) and no statistical differences was found between COVID-19^{pos} ARDS^{pos} and COVID-19^{pos} ARDS^{neg} (Fig. 3D).

Evolution of immune cell clusters between D0 and D7 in COVID-19 patients defines high-risk clinical grade

We performed mass cytometry analysis for 21 patients at day 7 of hospitalization, including 7 COVID-19^{neg} ARDS^{pos}, 8 COVID-19^{pos} ARDS^{pos}, and 6 COVID^{pos} ARDS^{neg} patients, in order to follow up the kinetic of PBMC phenotypic alterations. The 42 samples (21 at day 0 and 21 at day 7) were parsed by correspondence analysis using, as a variable, the abundance of myeloid and lymphoid clusters (Fig. 4A). The first and second dimensions of the correspondence analysis explained 85.1 % and 9 % of the differences acquired between D0 and D7. The first dimension captured the difference between D0 and D7 only for COVID-19^{pos} ARDS^{pos} ($P < 0.01$) (Fig. 4A). Because of the limited number of samples, only a trend was observed for COVID^{pos} ARDS^{neg} ($P = 0.062$). The top-five enriched populations accounting for the differences between D0 and D7 for COVID-19^{pos} ARDS^{pos} patients were Mo11, Mo181, T8_113, T4_34, and NK_197, corresponding

to an enrichment in non-classical monocytes (CD14^{low}CD16^{high}CD64^{low}CD36^{low}S100A9^{high}), in M-MDSC-like (HLA-DR^{low}S100A9^{high}), in effector memory CD127^{high} T8 cells, in T4 naïve cells, and in Ki-67^{high} proliferating NK cells. These 5 cell subsets were integrated in an immune score combining their fold change between D0 and D7. To define the relevance of this immune score in discriminating COVID-19 patients with unfavorable prognosis, we built a clinical score as the sum of events occurring during ICU stay (thromboembolic, ICU-acquired infection, septic shock, renal failure, and deaths) (Table 1). Interestingly, both the clinical and the immune scores were found correlated in severe COVID-19 patients, irrespectively of their ARDS status (Spearman R = 0.71; P = 0.006) (Fig. 4B). Finally, we analyzed changes between D0 and D7 of genes involved in IFN pathway. We found and upregulation of *IFNAR1* and *IFNAR2* during time in COVID^{pos}ARDS^{pos} (Fig. S5A). Conversely, evolution of IFN type I target genes (*ISG15*, *IFI27*, *IFI44L*, *RSAD2*, and *IFIT1*) revealed a specific downregulation in COVID^{pos}ARDS^{pos} samples. Interestingly, both IFNAR score and type I IFN score, obtained by combining the expression of IFN receptors and targets, respectively, presented a trend of correlation with the immune score (Fig. S5B), and the type I IFN score was significantly correlated with the CD169 expression (Fig. S5C).

Discussion

Immune response to COVID-19 infection has been recently intensively studied at both transcriptomic and proteomic levels. However, most studies focused on either the lymphoid^{19,22,24} or the myeloid compartments,^{12,21,23} and only few performed a wide analysis of the circulating immune landscape,^{13,16,25,42,43} thus precluding the definition of complex patterns of immune parameter alterations associated with COVID-19 severity or physiopathology. Moreover, these studies were designed to identify differences in immune cell subsets frequencies between

COVID-19 patients and healthy donors, and eventually correlated with the severity of the disease, but did not include severe non-COVID-19 patients as controls, although critically ill patients were previously largely demonstrated to display immune reprogramming.⁴⁴ ARDS is a major adverse event occurring during ICU stay, leading to an overall mortality rate of 40 % to 60 %. Whether COVID-19 associated ARDS is clinically and biologically similar to other causes of ARDS remains controversial.^{45,46} To address this point, we characterized for the first time, by mass cytometry, the immune landscape in COVID-19-associated ARDS compared to other causes of ARDS. We demonstrated that an increase of CD169^{pos} monocytes, correlated with specific changes of T, plasma, and NK cell subsets, defines COVID-19-associated ARDS and is not found in bacteria-associated ARDS, suggesting a COVID-19 specific immune reprogramming.

The amplification of CD169^{pos} circulating monocytes has already been highlighted in the context of COVID-19,^{15,23,38,47} and is reminiscent of other inflammatory conditions found in viral infections, such as with Human Immunodeficiency Virus or Epstein-Barr Virus, in which the CD169 sialoadhesin is induced in an IFN-dependent manner on the surface of circulating monocytes.^{48,49} Consistent with the inflammatory response, we showed that the accumulation of CD169^{pos} monocytes in COVID-19^{pos} patients is positively correlated with an increase of plasmablasts and mature plasma cells, Th1-like CD8 effector T cells, cytotoxic mature NK cells, and activated CD4 effector memory T cells displaying a CTLA4^{high}PD1^{high} phenotype. CD169^{pos} activated monocytes were detected in mild disease,²³ and were proposed to rise rapidly and transiently in patients with COVID-19, in association with a high expression of IFN γ and CCL8.¹⁵ This could be due to the transient nature of this monocytic population, either losing CD169, being short-lived, or being recruited into tissues as CD169^{pos} macrophages, as suggested by the high expression of CCR2 on Mo243 and Mo180, the two monocyte subsets identified here

in COVID-19 patients, and the local inflammation and lung tissue destruction mediated by monocyte-derived macrophages in severe cases of SARS-CoV2 infections.^{50,51} Interestingly, we also found an upregulation of cytoplasmic S100A9 in monocyte subsets specifically amplified in COVID-19 patients irrespectively of their ARDS status. These data suggest that, in the early stage of the disease, monocytes could contribute to the burst of circulating calprotectin (S100A8/S100A9), recently proposed to contribute to the secondary cytokine release syndrome described in severe COVID-19 and attributed to neutrophils.²¹ Despite phenotypic alterations, our data revealed a specific alteration of the response to type I IFN in COVID-19^{pos} *versus* COVID-19^{neg} ARDS patients after short stay in ICU, with an upregulation of IFN receptors without induction of IFN target genes. These results are reminiscent of the demonstration that deficiency of type I IFN pathway is associated with poor outcome in COVID-19 patients.^{52,53}

Whereas a seroconversion score was recently associated with huge modifications immune parameters reflecting B, T, and NK cell function in non-ICU COVID patients,⁵⁴ our ICU patients clearly stand at a later stage of the disease, with 22 out of 29 already carrying neutralizing antibodies at D0. It is thus highly unlikely that the differential evolution of monocytic markers identified between D0 and D7 in our study could be attributable to seroconversion.

Within severe COVID-19 patients, we detected no significant differences between ARDS^{pos} and ARDS^{neg} immune profiles, indicating a specificity of the phenotype induced by SARS-CoV2 infection, irrespectively of the respiratory complications. While most published studies showed differences between mild and severe COVID-19 diseases, some of their conclusions might be obscured by the fact that ARDS by itself, mechanical ventilation, and/or nonspecific treatments might impact immune parameters.⁵⁵ A strength of our study comparing two groups of severe COVID-19 patients with or without ARDS is to highlight features directly related to the viral infection rather than to its respiratory complications or their treatment. Importantly, our cohort

was homogeneous regarding treatment with in particular no immunosuppressive therapy at the time of sampling.

The small size of our cohort did not allow us to pinpoint a mortality prognostic factor based on our phenotypic data. However, we identified a specific immune pattern associated with the occurrence of the major adverse clinical events (thrombosis, nosocomial infection, septic shock, acute renal failure, and death) described in COVID-19 and combined as a clinical score. In particular, an increase of non-classical $CD14^{low}CD16^{pos}$ monocytes (Mo11), and $CD14^{pos}HLA-DR^{low}$ M-MDSC-like (Mo181), both not expressing CD169, are markers of adverse events. This suggests that besides the early increase of $CD169^{pos}$ monocytes in all COVID-19 patients associated with T-cell dysfunctions, the immunological response to SARS-CoV2 infection features multiple alterations of monocytic subsets reflecting the severity of the disease. Consistent with these data, it was shown that $CD14^{pos}HLA-DR^{low}$ cells were increased in critical COVID-19 patients,^{21,26,56-58} while $CD14^{low}CD16^{pos}$ monocytes, able to migrate to the lung, were correlated with the length of stay in ICU.^{15,23,59} Altogether, our study correlates the accumulation of non-classical monocytes and M-MDSCs occurring during the first days of ICU to adverse events.

Limitations of Study

Besides the low number of included patients, our study has some limitations. By focusing on severe patients with and without ARDS, we cannot make conclusions about phenotypic changes in mild and moderate diseases. The analysis would also benefit from comparison with other virus-associated ARDS. We thus analyzed a published dataset of flu-like illness and COVID patients, analyzed by mass cytometry.²¹ Interestingly, by using CellCnn, we were able to define a filter that accurately discriminate flu-like illness from COVID samples, suggesting immune differences between both diseases (Fig. S4). Moreover, since the mass cytometry was conducted on PBMCs,

we lack information on the neutrophil lineage, which appears affected in COVID-19 disease.²¹ It would also be interesting to link these data with *in situ* data from lung tissue samples and bronchoalveolar lavages. Unfortunately, at the time of the study, bronchoalveolar fluid collection was not allowed in our institution for patients positive for SARS-CoV2. However, our detailed analysis of circulating immune cells shows that immune monitoring of severe COVID-19 patients brings interesting prognostic biomarkers independently of their clinical classification in ARDS^{pos} versus ARDS^{neg}. Moreover, we demonstrated that at the biological level, COVID-19 associated ARDS is different from other causes of ARDS, and might benefit from personalized therapy in addition to standard ARDS management.^{23,60}

Acknowledgments: We thank all donors, families, and surrogates, as well as the medical personnel in charge of patient care. We thank Catherine Blanc and Aurelien Corneau, from the CyPS core facility at Sorbonne University, Paris for access to the Helios mass cytometer.

Funding: This work was supported by the University hospital of Rennes, CFTR² (COVID-19 Fast Track Recherche Rennes) grant (to F.R.) and by the Fondation pour la Recherche Médicale (FRM) and the Agence Nationale de la Recherche (ANR), Flash Covid-19 joint grant (HARMONICOV to M.Cog.).

Author contributions: Conceptualization, M.R., F.R., M.Le, J.M.T., M.Cog., and K.T.; Methodology, M.R., S.L.G, J.D., and K.T; Formal analysis, M.R., J.Fer., S.L., and S.C.; Investigation, S.L.G., J.D., C.M., M.G., N.B., C.V., M.La., I.B., and M.Cor.; Resources, F.R., M.Le., B.S, S.P., J.Feu., R.J., T.D.,V.K.T., and J.M.T.; Data curation, M.R., J.Fer. and F.R.; Writing - original draft preparation, M.R. and J.Fer.; Writing - review and editing, M.R., J.Fer., S.L.G., S.C., V.K.T., J.M.T., M.Cog., and K.T.; Visualization, M.R. and J.Fer.; Supervision, M.R. and K.T.; Project administration, M.R. and K.T.; Funding acquisition, F.R. and M.Cog.

Competing interests: J.Fer., F.R., S.L.G., J.D., M.Le., M.G., N.B., C.V., M.La., I.B., M.Cor., A.V., C.M., B.S., S.L., S.P., J.Feu., R.J., T.D., and M. Cog. declare no competing interest. M.R., S.C., V.K.T., J.M.T., and K.T. are the inventors of a patent EP 20305642.9 “A method for early detection of propensity to severe clinical manifestations Methods” submitted June 11th 2020 under University hospital of Rennes and Scailyte AG names.

Fig. 1: SARS-CoV2 induces specific phenotype of circulating immune cells

CellCnn analysis performed on single cells from myeloid (top) and lymphoid (bottom) panels on 39 samples at admission (Day 0) (COVID-19^{neg} [n = 9] and COVID-19^{pos} [n = 30]). **(A)** Frequencies of cells discovered by the best-performing CellCnn filter in COVID-19^{neg} (blue) and COVID-19^{pos} (orange) patients for each panel. Mann-Whitney tests, ****P < 0.0001. **(B)** Cells defined by the best-performing CellCnn filters enrichment shown on tSNE and representative markers for each panel (CD14 and CD38 [see additional markers in Fig. S2]).

Fig. 2: CD169 monocytes are enriched in SARS-CoV2 infected patients

(A) Heatmap of the 15 monocyte metaclusters defined after FlowSOM analysis. **(B)** Relative abundance of metaclusters among monocytes for each patient and hierarchical clustering of COVID-19^{neg}ARDS^{pos} (n=12, green), COVID-19^{pos}ARDS^{pos} (n=13, blue), and COVID-19^{pos}ARDS^{neg} (n=17, red). **(C)** Abundance of metaclusters differentially expressed between groups, among singlet cell analyzed. **(D)** Expression of the corresponding markers (mean metal intensity) for background (gray), Mo11 and Mo181 (orange), and Mo243 and Mo180 (blue) metaclusters. **(E)** Abundance of Mo22, Mo180, and Mo243 and expression of CD169 (Box and Whiskers with 10 and 90 percentile). **(F)** UMAP from scRNAseq of COVID-19 patients (COVID-19) and healthy donors (healthy) highlighting CD14 and CD169 expression (data obtained from Wilk et al.²⁵) Kruskal-Wallis test with Dunn's multiple comparison correction, *P < 0.05, **P < 0.01, ***P < 0.001.

Fig.3: Monocyte metaclusters enriched in COVID-19 are correlated with effector memory T cells and plasma cells

(A) Correlation between Mo180 and Mo243 and lymphoid clusters (see heatmap for all lymphoid clusters and markers in Fig. S2) from all patients at D0 (COVID-19^{neg}ARDS^{pos} [n=12], COVID-19^{pos}ARDS^{pos} [n=13], and COVID-19^{pos}ARDS^{neg} [n=17]). Only strong correlations (Spearman $R > 0.5$ or $R < -0.5$ and $P < 0.01$) are shown (see all significant correlations [$P < 0.05$] in Fig. S2 and Table S4). (B) Heatmap showing marker expression for the lymphoid clusters (Spearman $R > 0.5$ or $R < -0.5$ and $P < 0.001$) strongly correlated with Mo180 and Mo243 (see heatmap for all clusters and markers in Fig. S2). (C) Abundance of lymphoid clusters differentially expressed between groups, among singlet cells analyzed. Kruskal-Wallis test with Dunn's multiple comparison correction, * $P < 0.05$, ** $P < 0.01$, *** $P < 0.001$ [see all clusters in Fig. S2]). (D) Two first dimensions of correspondence analysis accounting for 84 % of the association between immune clusters differentially expressed between groups (n= 4 monocyte- and n=22 lymphoid-clusters), and patients. For clarity, patients and immune cells are shown on 2 different plots. Dimensions 1 and 2 coordinates are compared between groups of patients. Kruskal-Wallis test with Dunn's multiple comparison correction, **** $P < 0.0001$.

Fig. 4: Evolution of immune cell subsets between D0 and D7, defines high-risk clinical grade COVID-19 patients

(A) Two first dimension of correspondence analysis accounting for 94.1% of the association between immune clusters differentially expressed between groups (n= 4 monocyte and n=22 lymphoid clusters), and patients for which a follow-up of 7 days was available (COVID-19^{neg}ARDS^{pos} [n=7], COVID-19^{pos}ARDS^{pos} [n=8], and COVID-19^{pos}ARDS^{neg} [n=6]). For clarity, patients and immune cells are shown on 2 different plots. Dimensions 1 and 2 coordinates were compared between D0 and D7 for each group of patients. Wilcoxon matched-pairs signed rank

tests, $**P < 0.01$. **(B)** Spearman correlation between immune and clinical score for COVID-19^{pos} patients (ARDS^{pos} [n=8] and ARDS^{neg} [n=6]).

Journal Pre-proof

Table 1: Patients' characteristics for the cohort 1

| | COVID-19 ^{neg} | COVID-19 ^{pos} | COVID-19 ^{pos} |
|---|-------------------------|-------------------------|-------------------------|
| | ARDS ^{pos} | ARDS ^{pos} | ARDS ^{neg} |
| Patients D0/D7, n | 12/7 | 13/8 | 17/6 |
| Age, median (IQR) | 62 (48.2-66.7) | 59 (53.5-67.5) | 55 (46-67) |
| Male, n (%) | 7 (58) | 10 (77) | 12 (71) |
| ICU/Clinical ward, n | 12/0 | 13/0 | 11/6* |
| SAPS II, median (IQR) | 44.5 (29.2-59.2) | 33 (19.5-39.5) | 22 (13-28)* |
| Length of stay in ICU, median (IQR) | 11.5 (4.5-18.7) | 15 (11-54) | 2 (1-2)** |
| Length of stay in Hospital, median (IQR) | 18 (7-30.5) | 22 (15-62.5) | 9 (7.5-13) |
| Comorbidities | | | |
| BMI, median (IQR) | 26.4 (19.5-28.4) | 28.6 (25-32) | 28.1 (22.3-32.1) |
| Chronic cardiovascular disease, n (%) | 1 (8.3) | 3 (23) | 1 (5.8) |
| Diabetes, n (%) | 2 (16.7) | 3 (23) | 1 (5.8) |
| Chronic respiratory disease, n (%) | 1 (8.3) | 0 (0) | 0 (0) |
| Chronic kidney disease, n (%) | 0 (0) | 2 (15.4) | 0 (0) |
| Cancer, n (%) | 3 (25) | 0 (0) | 0 (0) |
| Severity criteria | | | |
| Maximal O ₂ (L/min), median (IQR) | 10 (7.5-15) | 14 (9.2-15) | 3 (2-5) |
| Invasive ventilation, n (%) | 12 (100) | 13 (100) | 0 (0) |
| PaO ₂ /FiO ₂ , median (IQR) | 116.5 (75.2-161.9) | 106 (95.5-240) | 313 (218.5-340.3) |
| Events occurring during follow up | | | |
| Thromboembolic, n (%) | 4 (33.3) | 4 (30.8) | 1 (5.8) |
| ICU-acquired infections, n (%) | 2 (16.7) | 7 (53.8) | 0 (0) |
| Septic shock, n (%) | 3 (25) | 2 (15.4) | 0 (0) |
| Renal failure, n (%) | 5 (41.7) | 8 (61.5) | 0 (0) |
| Deaths, n (%) | 4 (33.3) | 1 (7.7) | 0 (0) |

*: all patients except 1 required O₂ at > 2 L/mn at admission; **: For patients in ICU; n: number; IQR: interquartile range; SAPS II: simplified acute physiology score

STAR*METHODS**KEY RESOURCES TABLE**

| REAGENT or RESOURCE | SOURCE | IDENTIFIER |
|----------------------------|-----------------|--------------------------------------|
| Antibodies | | |
| CD11c (3.9), Purified | BioLegend | Cat# 301602, RRID:AB_314172 |
| CD33 (WM53), Purified | BioLegend | Cat# 303402, RRID:AB_314346 |
| CD209 (9E9A8), Purified | BioLegend | Cat# 330102, RRID:AB_1134253 |
| CD14 (M5E2), Purified | BioLegend | Cat# 301802, RRID:AB_314184 |
| CD123 (6H6), Purified | BioLegend | Cat# 306002, RRID:AB_314576 |
| CD21 (Bu32), Purified | BioLegend | Cat# 354902, RRID:AB_11219188 |
| CD192 (K036C2), Purified | BioLegend | Cat# 357202, RRID:AB_2561851 |
| CD163 (GHI/61), Purified | BioLegend | Cat# 333602, RRID:AB_1088991 |
| CD36 (5-271), Purified | BioLegend | Cat# 336202, RRID:AB_1279228 |
| CD86 (IT2.2), Purified | BioLegend | Cat# 305402, RRID:AB_314522 |
| CD169 (7-239), Purified | BioLegend | Cat# 346002, RRID:AB_2189031 |
| CD274 (29E.2A3), Purified | BioLegend | Cat# 329719, RRID:AB_2565429 |
| CD254 (MIH24), Purified | BioLegend | Cat# 347501, RRID:AB_2044062 |
| CD106 (EPR5047), Purified | Abcam | Cat# ab134047, RRID:AB_2721053 |
| CD3 (UCHT1), Purified | BioLegend | Cat# 300402, RRID:AB_314056 |
| CD49a (TS2/7), Purified | BioLegend | Cat# 328302, RRID:AB_1236385 |
| gp38 (REA446), Purified | Miltenyi Biotec | Cat# 130-107-017, RRID:AB_2653261 |
| CD80 (2D10), Purified | BioLegend | Cat# 305202, RRID:AB_314498 |
| CD34 (581), Purified | BioLegend | Cat# 343502, RRID:AB_1731898 |
| CD1a (HI149), Purified | BioLegend | Cat# 300102, RRID:AB_314016 |
| CX3CR1 (2A9-1), Purified | BioLegend | Cat# 341602, RRID:AB_1595422 |
| CD32 (FUN-2), Purified | BioLegend | Cat# 303202, RRID:AB_314334 |
| CD54 (HA58), Purified | BioLegend | Cat# 353102, RRID:AB_11204426 |
| CD195 (J418F1), Purified | BioLegend | Cat# 359102, RRID:AB_2562457 |
| CD206 (15-2), Purified | BioLegend | Cat# 321102, RRID:AB_571923 |
| S100A9 (A15105J), Purified | BioLegend | Cat# 600302, RRID:AB_2721747 |

| | | |
|---------------------------|--------------------------|-------------------------------------|
| CD45RA (HI100), Purified | BioLegend | Cat# 304102, RRID:AB_314406 |
| CD172a (15-414), Purified | BioLegend | Cat# 372102, RRID:AB_2629807 |
| CD68 (Y1/82A), Purified | BioLegend | Cat# 333802, RRID:AB_1089058 |
| CD11b (ICRF44), 209Bi | Fluidigm | Cat# 3209003, RRID:AB_2687654 |
| CD8a (RPA-T8), Purified | BioLegend | Cat# 301053, RRID:AB_2562810 |
| CD4 (RPA-T4), Purified | BioLegend | Cat# 300502, RRID:AB_314070 |
| CD25 (BC96), Purified | BioLegend | Cat# 302602, RRID:AB_314272 |
| CD38 (HIT2), Purified | BioLegend | Cat# 303502, RRID:AB_314354 |
| CXCR3 (G025H7), Purified | BioLegend | Cat# 353733, RRID:AB_2563724 |
| FoxP3 (259D/C7), Purified | BD Biosciences | Cat# 560044, RRID:AB_1645589 |
| CD7 (CD7-6B7), Purified | BioLegend | Cat# 343111, RRID:AB_2563761 |
| Gata-3 (TWAJ), Purified | Thermo Fisher Scientific | Cat# 14-9966-82, RRID:AB_1210519 |
| CCR7 (G043H7), Purified | BioLegend | Cat# 353237, RRID:AB_2563726 |
| CCR6 (G034E3), Purified | BioLegend | Cat# 353427, RRID:AB_2563725 |
| CD27 (O323), Purified | BioLegend | Cat# 302802, RRID:AB_314294 |
| CD10 (HI10a), Purified | BioLegend | Cat# 312223, RRID:AB_2562828 |
| CD117 (104D2), Purified | BioLegend | Cat# 105814, RRID:AB_313223 |
| CCR4 (L291H4), Purified | BioLegend | Cat# 359402, RRID:AB_2562364 |
| CD161 (HP-3G10), Purified | BioLegend | Cat# 339919, RRID:AB_2562836 |
| CD185 (J252D4), Purified | BioLegend | Cat# 356902, RRID:AB_2561811 |
| RORgt (AFKJS-9), Purified | Thermo Fisher Scientific | Cat# 14-6988-82, RRID:AB_1834475 |
| CD294 (BM16), Purified | BioLegend | Cat# 350102, RRID:AB_10639863 |
| LAG-3 (7H2C65), Purified | BioLegend | Cat# 369202, RRID:AB_2616877 |
| CTLA-4 (L3D10), Purified | BioLegend | Cat# 349902, RRID:AB_10642827 |
| PD-1 (EH12.2H7), Purified | BioLegend | Cat# 329941, RRID:AB_2563734 |
| Tim-3 (F38-2E2), Purified | BioLegend | Cat# 345019, RRID:AB_2563790 |
| CD127 (A019D5), Purified | BioLegend | Cat# 351337, RRID:AB_2563715 |
| Bcl-6 (k112-91), Purified | BD Biosciences | Cat# 561520, |

| | | |
|--|---|------------------------------------|
| | | RRID:AB_10713172 |
| T-bet (4B10), Purified | BioLegend | Cat# 644825, RRID:AB_2563788 |
| CD45RO (UCHL1), Purified | BioLegend | Cat# 304239, RRID:AB_2563752 |
| CD56 (HCD56), Purified | BioLegend | Cat# 318302, RRID:AB_604092 |
| Ki-67 (Ki-67), Purified | BioLegend | Cat# 350523, RRID:AB_2562838 |
| CD44 (BJ18), Purified | BioLegend | Cat# 338802, RRID:AB_1501199 |
| CD45 (HI30), 89Y | Fluidigm | Cat# 3089003, RRID:AB_2661851 |
| CD326 (9C4), Purified | BioLegend | Cat# 324229, RRID:AB_2563742 |
| CD19 (HIB19), Purified | BioLegend | Cat# 302202, RRID:AB_314232 |
| HLA-DR (10.1), Purified | BioLegend | Cat# 307602, RRID:AB_314680 |
| CD31 (WM59), Purified | BioLegend | Cat# 303127, RRID:AB_2563740 |
| CD16 (B73.1), Purified | BioLegend | Cat# 360702, RRID:AB_2562693 |
| CD64 (L243), Purified | BioLegend | Cat# 305029, RRID:AB_2563759 |
| Biological Samples | | |
| Chemicals, Peptides, and Recombinant Proteins | | |
| EQ Four Element Calibration Beads | Fluidigm | Cat# 201078 |
| Antibody Stabilizer PBS | Candor Bioscience | Cat# 131050 |
| Bond-Breaker™ TCEP Solution | Thermo Fisher Scientific | Cat# 77720 |
| Cell-ID™ Intercalator-Ir | Fluidigm | Cat# 201192B |
| Cell-ID™ Cisplatin-198Pt | Fluidigm | Cat# 201198 |
| Cell Acquisition Solution | Fluidigm | Cat# 201240 |
| Critical Commercial Assays | | |
| Transcription factor staining buffer set | Miltenyi Biotec | Cat# 130-122-981 |
| Maxpar® X8 Multimetal Antibody Labeling Kit | Fluidigm | Cat# 201300 |
| Preamp Master Mix | Fluidigm | Cat# 100-5580 |
| Reverse Transcription Master Mix | Fluidigm | Cat# 100-6298 |
| TaqMan Universal PCR Master Mix (2X) | Life Technologies | Cat# PN 4304437 |
| 96.96 DNA Binding Dye Sample/Loading Kit—10 IFCs | Fluidigm | Cat# BMK-M10-96.96-EG |
| Deposited Data | | |
| CyTOF data | Chevrier et al, Cell Reports Medicine, 2021 | DOI: 10.1016/j.xcrm.2020.100166 |

| | | |
|--|---|---|
| scRNAseq sata | Wilk et al, Nat Med, 2020 | DOI: 10.1038/s41591-020-0944-y |
| Cytof data | Schulte-Schrepping et al, Cell, 2020 | DOI: 10.1016/j.cell.2020.08.001 |
| Cytof data | This paper | DOI: 10.17632/xg9k72r5rt.1 |
| Cytof data | This paper | DOI: 10.17632/c29frc3y6s.1 |
| Clinical data | This paper | DOI: 10.17632/5n8df8jvk4.1 |
| Oligonucleotides | | |
| IFIT1: interferon induced protein with tetratricopeptide repeats 1 | TaqMan® Assays, ThermoFisher Scientific | Hs03027069_s1 |
| IFNAR1: interferon alpha and beta receptor subunit 1 | TaqMan® Assays, ThermoFisher Scientific | Hs01066116_m1 |
| ISG15: ISG15 ubiquitin-like modifier | TaqMan® Assays, ThermoFisher Scientific | Hs01921425_s1 |
| IFI27: interferon alpha inducible protein 27 | TaqMan® Assays, ThermoFisher Scientific | Hs01086373_g1 |
| IFI44L: interferon induced protein 44 like | TaqMan® Assays, ThermoFisher Scientific | Hs00915287_m1 |
| RSAD2: radical S-adenosyl methionine domain containing 2 | TaqMan® Assays, ThermoFisher Scientific | Hs00369813_m1 |
| IFNAR2: interferon alpha and beta receptor subunit 2 | TaqMan® Assays, ThermoFisher Scientific | Hs01022059_m1 |
| ELF1: E74-like factor 1 (ets domain transcription factor) | TaqMan® Assays, ThermoFisher Scientific | Hs00152844_m1 |
| Software and Algorithms | | |
| CellCnn, ScaiVision platform | Scailte AG | version 0.3.6 |
| R | https://www.cran.r-project.org | v3.6.3 |
| Premessa (R package) | https://github.com/ParkerICI/premessa | premessa 0.2.6 |
| viSNE (Cytobank) | Amir et al, Nat Biotechnol (2014) | NA |
| FlowSOM (Cytobank) | Van Gassen et al, Cytometry A (2015) | NA |
| Rstudio | https://rstudio.com/ | v1.2.5033 |
| pheatmap (R package) | https://cran.r-project.org/package=pheatmap | v1.0.12 (CRAN) |
| Cytobank | Kotecha et al., 2010 https://www.cytobank.org | https://doi.org/10.1002/0471142956.cy1017s53 |
| Kaluza | Beckman Coulter | v2.1.00002 |
| Prism (software) | https://www.graphpad.com | v8 |

RESOURCE AVAILABILITY

Lead contact

Further information and requests for resources and reagents should be directed to and will be fulfilled by the Lead Contact, Mikael Roussel (mikael.roussel@chu-rennes.fr)

Material Availability

The study did not generate new unique reagents.

Data and Code Availability

Additional Supplemental Items are available from Mendeley Data at <http://dx.doi.org/10.17632/xg9k72r5rt.1>, <http://dx.doi.org/10.17632/c29frc3y6s.1>, and <http://dx.doi.org/10.17632/5n8df8jvk4.1>

EXPERIMENTAL MODEL AND SUBJECT DETAILS

Patients

This study was performed in the infectious diseases department and intensive care unit (ICU) at Rennes University Hospital. The study design was approved by our ethic committee (CHU Rennes, n°35RC20_9795_HARMONICOV, ClinicalTrials.gov Identifier: NCT04373200) and informed consent was obtained from patients in accordance with the Declaration of Helsinki. Patients with malignancy, HIV-infected patients, and patients with preexisting immune disorders or receiving immunosuppressive agents were excluded. The presence of SARS-CoV-2 in respiratory specimens (nasal and pharyngeal swabs or sputum) was detected by real-time reverse transcription polymerase chain reaction (RT-PCR) methods (TaqPath COVID-19, ThermoFisher).

Cohort 1: Peripheral blood was collected in tubes containing lithium heparin from COVID-19^{neg}ARDS^{pos}, COVID-19^{pos}ARDS^{pos}, and COVID-19^{pos}ARDS^{neg} patients. Peripheral blood

samples were drawn at D0 and D7. PBMC were isolated from whole blood using ficoll before cryopreservation. All patients provided written informed consent. The following data were recorded: gender, age, preexisting chronic kidney disease and acute kidney failure during the ICU stay,⁶¹ preexisting chronic heart failure,⁶² Body Mass Index (BMI), SAPS II at admission,⁶³ duration of mechanical ventilation, length of hospital stay, and outcome (alive or dead) on day 7, day 30 and day 90. The occurrence of nosocomial infection, defined following CDC criteria as previously described,⁶⁴ was also recorded during hospital stay. For each patient, a clinical score was built to summarize the occurrence of adverse clinical events frequently encountered during hospitalization.^{64,65} Each of the following events: thromboembolic events, nosocomial infection, septic shock, acute renal failure, and death counting as one point, the score varies from 0 (no adverse events) to 5. Patients' characteristics for cohort 1 are reported in Table 1 and Table S1.

Cohort 2: Same inclusion criteria were applied to cohort 2. Only patients at D0 were included. Patients' characteristics for cohort 1 are reported in Table S1 and Table S2.

METHODS DETAILS

Mass cytometry analysis

PBMC from patients were thawed. Briefly, cells were stained 5 minutes in RPMI supplemented with 0.5 μ M Cisplatin Cell-ID™ (Fluidigm, San Francisco, CA) in RPMI 1640 before washing with 10% FCS in RPMI 1640. Cell pellets were resuspended in 80 μ l of 0.5% BSA in PBS. Then 60 μ l of each surface staining cocktail, lymphoid or myeloid, were added to 40 μ l of resuspended cells. After staining, cells were washed in 0.5% BSA in PBS before fixation/permeabilization with the transcription factor staining buffer set (Miltenyi, Bergisch-Gladbach, Germany). Then 60 μ l of each surface staining cocktail, lymphoid or myeloid, were added to 40 μ l of resuspended

cells in Perm Buffer. The panel of antibodies is listed in Table S3 and in Key Resources Table. After intracellular staining, cells were washed twice before staining in DNA intercalator solution (2.5% Paraformaldehyde, 1:3200 Cell-ID™ Intercalator-Ir (Fluidigm, San Francisco, CA) in PBS). Samples were cryopreserved at -80°C until acquisition on Helios™ System (Fluidigm, San Francisco, CA).

Antibodies and reagents

Purified antibodies for mass cytometry were obtained in carrier/protein-free buffer and then coupled to lanthanide metals using the MaxPar antibody conjugation kit (Fluidigm Inc.) according to manufacturer's recommendations. Following the protein concentration determination by measurement of absorbance at 280 nm and titration on positive controls, the metal-labeled antibodies were diluted in Candor PBS Antibody Stabilization solution (Candor Bioscience, Germany) for long-term storage at 4°C. Antibodies used are listed in Table S3 and Key Resources Table.

Quantitative real-time polymerase chain reaction

Total RNA was extracted from PAXgene blood RNA kit (Qiagen, Valencia, CA) using a Hamilton Microlab STARlet Automated Handler (Atlantic Lab Equipment, Beverly, MA). cDNA was then prepared using Reverse Transcription Master Mix (Fluidigm Sunnyvale, CA) and gene expression preamplification was performed with Fluidigm Preamp Master Mix and Taqman Assays (Invitrogen, Thermo Fisher Scientific Inc, Carlsbad, CA, USA). After loading the reaction chambers using the integrated fluid circuit (IFC) HX controller from Fluidigm, the realtime PCR was performed in a BioMark HD system (Fluidigm Corp., USA) using single probe (FAM-MGB, reference: ROX) settings and GE 96x96 standard v1 protocol. Data processing took place using

the Fluidigm real-time PCR analysis software (v. 4.1.3). For each sample, the cycle threshold (CT) value for the gene of interest was determined and normalized to the housekeeping gene *ELF1*. The relative level of expression of each gene for each patient at D7 compared to D0 was assessed using the 2-ddCT method. For all D0 samples, the relative level of expression of each gene was assessed by 2-dCT method. Type I IFN response score was determined as Log₂ of the mean of the following genes: *ISG15*, *IFI27*, *IFI44L*, *RSAD2* and *IFIT*. IFNAR score was considered as Log₂ of the mean of the following genes: *IFNAR1* and *IFNAR2*.

Detection of SARS-CoV-2 neutralizing antibodies

The viral strain (RoBo strain), which was cultured on Vero-E6 cells (ATCC CRL-1586), used for the nAb assay was a clinical isolate obtained from a nasopharyngeal aspirate of a patient HOS at the University Hospital of Saint-Etienne for severe COVID-19. The strain was diluted in Dulbecco's modified Eagle's medium–2% fetal calf serum in aliquots containing 100–500 tissue culture infectious doses 50% (TCID₅₀) per ml. Each serum specimen was diluted 1:10 and serial twofold dilutions were mixed with an equal volume (100 µL each) of virus. After gentle shaking for 30 min at room temperature, 150 µL of the mixture was transferred to 96-well microplates covered with Vero-E6 cells. The plates were then placed at 37°C in a 5% CO₂ incubator. Measurements were obtained microscopically 5–6 days later when the cytopathic effect of the virus control reached ~100 TCID₅₀/150 µL. The serum was considered to have protected the cells if >50% of the cell layer was preserved. The neutralizing titer is expressed as the inverse of the higher serum dilution that protected the cells.

QUANTIFICATION AND STATISTICAL ANALYSIS

Mass Cytometry Preprocessing

After acquisition, intrafile signal drift was normalized and .fcs files were obtained using CyTOF software. To diminish batch effects, all files were normalized on EQ Beads (Fluidigm Sciences) using the *premesa* R package (<https://github.com/ParkerICI/premesa>). Files were then uploaded to the Cytobank cloud-based platform (Cytobank, Inc.). Data were first arcsinh-transformed using a cofactor of 5. For all files, live single cells were selected by applying a gate on DNA1 vs. DNA2 followed by a gate on DNA1 vs. Cisplatin, then beads were removed by applying a gate on the beads channel (Ce140Di) vs. DNA.1 Normalized, transformed and gated values were exported as FCS files.

CellCnn analysis

Identification of a Covid-19-specific cell-identity signature was carried out using the CellCnn algorithm,³⁵ implemented in Pytorch in the ScaiVision platform (version 0.3.6, © Scailyte AG). Briefly, this is a supervised machine learning algorithm that trains a convolutional neural network with a single layer to predict sample-level labels using single-cell data as inputs. Data from each CyTOF panel was analyzed separately, in each case using all measured protein markers to train a series of CellCnn networks with varying hyperparameters. Each sample was given a label corresponding to the Covid-19 status of the patient from which the sample was drawn (positive or negative). To generate input data for training CellCnn, sub-samples of 2000 cells, termed multi-cell inputs (MCIs), were chosen randomly from each sample independently. For each training epoch, 2000 MCIs from each label class (Covid-19^{pos} or Covid-19^{neg}) were presented to the network in random order. During training, 30 % of the samples were set aside for validation, chosen in a stratified manner to maintain the relative proportions of each class. 50 independent networks were generated for each CyTOF panel using hyperparameters randomly chosen from the following options: i) number of filters: (2, 3, 5, 7, and 10), ii) top-k pooling percentage: (1, 5,

10, 20, and 30), iii) dropout probability: (0.3, 0.4, and 0.6), iv) learning rate: (0.001, 0.003, and 0.01), and v) weight decay: (0.00001, 0.0001, 0.001, 0.01, and 0.1). Training was performed with a batch size of 50. Adam was used as an optimizer {kingma2015adam}, with a beta1 coefficient of 0.999 and a beta2 coefficient of 0.99. Each network was trained for a maximum of 50 epochs, or until the validation loss no longer decreased for 10 consecutive epochs. At the end of training, the weights from the epoch with lowest validation loss were returned. Representative filters were determined by clustering the filters from all networks achieving ≥ 90 % accuracy on the validation samples, then choosing the filter in each cluster with the minimum distance to all other filters in that cluster. For both CyTOF panels, a single representative filter showing the largest positive association with the Covid-19^{POS} label class was used to calculate cell-level filter response scores. Thresholds were set on the filter response scores to select Covid-19-associated cells by calculating the relative frequencies of selected cells in each sample at 100 different thresholds for each filter, then performing a logistic regression to predict sample labels. For each threshold, the data was first split in a stratified manner into a training set, comprising 60 % of samples, and a test set, comprising 40 % of samples. The logistic regression was performed on the training set, and the accuracy of resulting predictions was calculated on the test set. This procedure was performed 10 times, with randomly chosen training/test splits, and the mean of the resulting accuracies for each threshold was calculated. For the lymphoid panel, one threshold (9.63) achieved the highest accuracy and was set as the final threshold. For the myeloid panel, multiple thresholds achieved the same level of accuracy; the lowest of these (4.96) was set as the final threshold. The relative frequencies of cells in each sample with filter response scores greater than or equal to the respective thresholds were calculated and compared using a Wilcoxon rank-sum test.

viSNE, FlowSOM, and hierarchical clustering

We first performed a dimension reduction for both panels (i.e. myeloid and lymphoid) and all cleaned-up 63 files were first analyzed using viSNE, based upon the Barnes–Hut implementation of t-SNE. Equal downsampling was performed, based on the lowest event count in all files (lymphoid panel) or on the maximum total events allowed by Cytobank (myeloid panel). For the myeloid panel, the following parameters were used: perplexity = 45; iterations = 5000; theta = 0.5; all 37 channels selected. For the lymphoid panel the parameters were as follows: perplexity = 45; iterations = 7500; theta = 0.5; all 36 channels selected.

Then we applied a clustering method using the FlowSOM clustering algorithm. FlowSOM uses Self-Organizing Maps (SOMs) to partition cells into clusters based on their phenotype, and then builds a Minimal Spanning Tree (MST) to connect the nodes of the SOM, allowing the identification of metaclusters (i.e. group of clusters). We performed the FlowSOM algorithm on the previous viSNE results, using all events and panel channels, and the following parameters: clustering method = hierarchical consensus, iterations = 10, number of clusters = 256, number of metaclusters = 30. For both panels, each metacluster (containing a given number of clusters) was manually annotated based on his marker expression phenotype, his projection on the viSNE and his localization in the FlowSOM MST.

We first analyzed the myeloid panel. Out of 30 metaclusters defined by the FlowSOM approach, we identified 13 metaclusters with monocyte markers, other metaclusters contained other cell types, low count of cells or remaining doublets or dead cells. We visually identified 2 (Mo18 and Mo26) out of the 13 metaclusters that were heterogeneous. These 2 metaclusters were manually split into 2 new metaclusters (identified respectively as Mo180, Mo181 and Mo214, Mo243) (Fig. S1B). Thus, altogether we analyzed 15 metaclusters of myeloid cells. Regarding the lymphoid compartment, we noticed that FlowSOM defined metaclusters at the lineage level, thus

we retain all the 136 clusters included in 10 metaclusters of interest (i.e. containing lymphoid lineage markers) (Fig. S1C). All metaclusters and clusters phenotypes including their abundances and mean marker intensity were then exported from Cytobank for further analyses. Cytometry data was explored with Kaluza Analysis Software (Beckman Coulter). Hierarchical clustering and heatmaps were generated with R v3.6.3, using Rstudio v1.2.5033 and the pheatmap package.

Statistical analysis

Statistical analyses were performed with Graphpad Prism 8.4.3. P values were defined by a Kruskal-Wallis test followed by a Dunn's post-test for multiple group comparisons or by Wilcoxon matched-pairs signed rank tests as appropriate. Correlations were calculated using Spearman test. * $P < 0.05$, ** $P < 0.01$, *** < 0.001 , and **** $P < 0.0001$. Hierarchical clustering of the patients was performed using euclidean distance and complete clustering. Correspondence analysis was performed using the package factoshiny using as variable the abundance in cell subsets for each patient.

Supplementary Materials:

Figure S1. Description of the 2 cohorts of patients, CyTOF experimental design and data analysis pipeline. Related to Table 1 and Figures 1 and 2.

Figure S2. Supplemental data for cohort 1. Related to Figure 1B, 2 and 3.

Figure S3. CellCnn and FlowSOM analysis for cohort 2. Related to Figures 1, 2 and 3.

Figure S4. CellCnn analysis for Chevrier et al. (Cell Reports Medicine, 2021) data¹ and for Schulte-Schrepping et al. (Cell, 2020) data². Related to Figure 1.

Figure S5. IFN I pathway. Related to Figure 4.

Table S1. Clinical data (excel spreadsheet). Related to Table 1.

Table S2. Patients' characteristics for the cohort 2. Related to Table 1.

Table S3. Panel of antibodies. Related to STAR Methods.

Table S4. Spearman correlation between myeloid and lymphoid clusters. Related to Figure 3.

Journal Pre-proof

References and Notes:

- 1 Williamson EJ, Walker AJ, Bhaskaran K, Bacon S, Bates C, Morton CE *et al.* Factors associated with COVID-19-related death using OpenSAFELY. *Nature* 2020; **584**: 430–436.
- 2 Guan W-J, Ni Z-Y, Hu Y, Liang W-H, Ou C-Q, He J-X *et al.* Clinical Characteristics of Coronavirus Disease 2019 in China. *The New England journal of medicine* 2020; **382**: 1708–1720.
- 3 Huang C, Wang Y, Li X, Ren L, Zhao J, Hu Y *et al.* Clinical features of patients infected with 2019 novel coronavirus in Wuhan, China. *Lancet* 2020; **395**: 497–506.
- 4 Sepsis) CTG (Clinical R in IC and STG for GE and R in, Helms J, Tacquard C, Severac F, Leonard-Lorant I, Ohana M *et al.* High risk of thrombosis in patients with severe SARS-CoV-2 infection: a multicenter prospective cohort study. *Intens Care Med* 2020; **46**: 1089–1098.
- 5 Schultze JL, Aschenbrenner AC. COVID-19 and the human innate immune system. *Cell* 2021. doi:10.1016/j.cell.2021.02.029.
- 6 Chen G, Wu D, Guo W, Cao Y, Huang D, Wang H *et al.* Clinical and immunologic features in severe and moderate Coronavirus Disease 2019. *J Clin Invest* 2020; **130**: 2620–2629.
- 7 Jeannot R, Daix T, Formento R, Feuillard J, François B. Severe COVID-19 is associated with deep and sustained multifaceted cellular immunosuppression. *Intens Care Med* 2020; **46**: 1769–1771.
- 8 Libster R, Marc GP, Wappner D, Coviello S, Bianchi A, Braem V *et al.* Early High-Titer Plasma Therapy to Prevent Severe Covid-19 in Older Adults. *New Engl J Med* 2021; **384**: 610–618.
- 9 Arabi YM, Murthy S, Webb S. COVID-19: a novel coronavirus and a novel challenge for critical care. *Intens Care Med* 2020; **46**: 833–836.
- 10 Paassen J van, Vos JS, Hoekstra EM, Neumann KMI, Boot PC, Arbous SM. Corticosteroid use in COVID-19 patients: a systematic review and meta-analysis on clinical outcomes. *Crit Care* 2020; **24**: 696.
- 11 Ni Y-N, Chen G, Sun J, Liang B-M, Liang Z-A. The effect of corticosteroids on mortality of patients with influenza pneumonia: a systematic review and meta-analysis. *Crit Care* 2019; **23**: 99.
- 12 Agrati C, Sacchi A, Bordoni V, Cimini E, Notari S, Grassi G *et al.* Expansion of myeloid-derived suppressor cells in patients with severe coronavirus disease (COVID-19). *Cell Death Differ* 2020; **27**: 3196–3207.

- 13 Arunachalam PS, Wimmers F, Mok CKP, Perera RAPM, Scott M, Hagan T *et al.* Systems biological assessment of immunity to mild versus severe COVID-19 infection in humans. *Science* 2020; **369**: 1210–1220.
- 14 Chen Z, Wherry EJ. T cell responses in patients with COVID-19. *Nat Rev Immunol* 2020; **20**: 529–536.
- 15 Chevrier S, Zurbuchen Y, Cervia C, Adamo S, Raeber ME, Souza N de *et al.* A distinct innate immune signature marks progression from mild to severe COVID-19. *Cell Reports Medicine* 2021; **2**: 100166.
- 16 Hadjadj J, Yatim N, Barnabei L, Corneau A, Boussier J, Smith N *et al.* Impaired type I interferon activity and inflammatory responses in severe COVID-19 patients. *Science* 2020; **369**: 718–724.
- 17 Lucas C, Wong P, Klein J, Castro TBR, Silva J, Sundaram M *et al.* Longitudinal analyses reveal immunological misfiring in severe COVID-19. *Nature* 2020; **584**: 463–469.
- 18 Mann ER, Menon M, Knight SB, Konkel JE, Jagger C, Shaw TN *et al.* Longitudinal immune profiling reveals key myeloid signatures associated with COVID-19. *Sci Immunol* 2020; **5**: eabd6197.
- 19 Mathew D, Giles JR, Baxter AE, Oldridge DA, Greenplate AR, Wu JE *et al.* Deep immune profiling of COVID-19 patients reveals distinct immunotypes with therapeutic implications. *Science* 2020; **369**: eabc8511.
- 20 Ren X, Wen W, Fan X, Hou W, Su B, Cai P *et al.* Large-scale single-cell analysis reveals critical immune characteristics of COVID-19 patients. *Biorxiv* 2020; : 2020.10.29.360479.
- 21 Schulte-Schrepping J, Reusch N, Paclik D, Baßler K, Schlickeiser S, Zhang B *et al.* Severe COVID-19 Is Marked by a Dysregulated Myeloid Cell Compartment. *Cell* 2020; **182**: 1419–1440.e23.
- 22 Sekine T, Perez-Potti A, Rivera-Ballesteros O, Strålin K, Gorin J-B, Olsson A *et al.* Robust T Cell Immunity in Convalescent Individuals with Asymptomatic or Mild COVID-19. *Cell* 2020; **183**: 158-168.e14.
- 23 Silvin A, Chapuis N, Dunsmore G, Goubet A-G, Dubuisson A, Derosa L *et al.* Elevated Calprotectin and Abnormal Myeloid Cell Subsets Discriminate Severe from Mild COVID-19. *Cell* 2020; **182**: 1401-1418.e18.
- 24 Song J-W, Zhang C, Fan X, Meng F-P, Xu Z, Xia P *et al.* Immunological and inflammatory profiles in mild and severe cases of COVID-19. *Nature Communications* 2020; **11**: 3410.
- 25 Wilk AJ, Rustagi A, Zhao NQ, Roque J, Martinez-Colon GJ, McKechnie JL *et al.* A single-cell atlas of the peripheral immune response in patients with severe COVID-19. *Nature medicine* 2020; **26**: 1070–1076.

- 26 Giamarellos-Bourboulis EJ, Netea MG, Rovina N, Akinosoglou K, Antoniadou A, Antonakos N *et al.* Complex Immune Dysregulation in COVID-19 Patients with Severe Respiratory Failure. *Cell Host Microbe* 2020; **27**: 992-1000.e3.
- 27 Merad M, Martin JC. Pathological inflammation in patients with COVID-19: a key role for monocytes and macrophages. *Nat Rev Immunol* 2020; **20**: 355–362.
- 28 Ong EZ, Chan YFZ, Leong WY, Lee NMY, Kalimuddin S, Mohideen SMH *et al.* A Dynamic Immune Response Shapes COVID-19 Progression. *Cell host & microbe* 2020; **27**: 879-882.e2.
- 29 Reizine F, Lesouhaitier M, Gregoire M, Pinceaux K, Gacouin A, Maamar A *et al.* SARS-CoV-2-Induced ARDS Associates with MDSC Expansion, Lymphocyte Dysfunction, and Arginine Shortage. *J Clin Immunol* 2021; **41**: 515–525.
- 30 Mudd PA, Crawford JC, Turner JS, Souquette A, Reynolds D, Bender D *et al.* Distinct inflammatory profiles distinguish COVID-19 from influenza with limited contributions from cytokine storm. *Sci Adv* 2020; **6**: eabe3024.
- 31 Biasi SD, Meschiari M, Gibellini L, Bellinazzi C, Borella R, Fidanza L *et al.* Marked T cell activation, senescence, exhaustion and skewing towards TH17 in patients with COVID-19 pneumonia. *Nat Commun* 2020; **11**: 3434.
- 32 Biasi SD, Tartaro DL, Meschiari M, Gibellini L, Bellinazzi C, Borella R *et al.* Expansion of plasmablasts and loss of memory B cells in peripheral blood from COVID-19 patients with pneumonia. *Eur J Immunol* 2020; **50**: 1283–1294.
- 33 Vabret N, Britton GJ, Gruber C, Hegde S, Kim J, Kuksin M *et al.* Immunology of COVID-19: Current State of the Science. *Immunity* 2020; **52**: 910–941.
- 34 Ranieri VM, Rubenfeld GD, Thompson BT, Ferguson ND, Caldwell E, Fan E *et al.* Acute respiratory distress syndrome: the Berlin Definition. *JAMA : the journal of the American Medical Association* 2012; **307**: 2526–2533.
- 35 Arvaniti E, Claassen M. Sensitive detection of rare disease-associated cell subsets via representation learning. *Nat Commun* 2017; **8**: 14825.
- 36 Galli E, Hartmann FJ, Schreiner B, Ingelfinger F, Arvaniti E, Diebold M *et al.* GM-CSF and CXCR4 define a T helper cell signature in multiple sclerosis. *Nat Med* 2019; **25**: 1290–1300.
- 37 Krieg C, Nowicka M, Guglietta S, Schindler S, Hartmann FJ, Weber LM *et al.* High-dimensional single-cell analysis predicts response to anti-PD-1 immunotherapy. *Nature medicine* 2018; **9**: 2579–14.
- 38 Bedin A-S, Makinson A, Picot M-C, Mennechet F, Malergue F, Pisoni A *et al.* Monocyte CD169 Expression as a Biomarker in the Early Diagnosis of Coronavirus Disease 2019. *J Infect Dis* 2020; **223**: 562–567.

- 39 Bourgoin P, Soliveres T, Barbaresi A, Loundou A, Belkacem IA, Arnoux I *et al.* CD169 and CD64 could help differentiate bacterial from CoVID-19 or other viral infections in the Emergency Department. *Cytom Part A* 2021. doi:10.1002/cyto.a.24314.
- 40 Ortilon M, Coudereau R, Cour M, Rimmelé T, Godignon M, Gossez M *et al.* Monocyte CD169 expression in COVID-19 patients upon intensive care unit admission. *Cytom Part A* 2021. doi:10.1002/cyto.a.24315.
- 41 Chevrier S, Levine JH, Zanotelli VRT, Silina K, Schulz D, Bacac M *et al.* An Immune Atlas of Clear Cell Renal Cell Carcinoma. *Cell* 2017; **169**: 736-738.e18.
- 42 Kuri-Cervantes L, Pampena MB, Meng W, Rosenfeld AM, Ittner CAG, Weisman AR *et al.* Comprehensive mapping of immune perturbations associated with severe COVID-19. *Sci Immunol* 2020; **5**: eabd7114.
- 43 Laing AG, Lorenc A, Barrio I del M del, Das A, Fish M, Monin L *et al.* A dynamic COVID-19 immune signature includes associations with poor prognosis. *Nat Med* 2020; **26**: 1623–1635.
- 44 Delano MJ, Ward PA. The immune system's role in sepsis progression, resolution, and long-term outcome. *Immunol Rev* 2016; **274**: 330–353.
- 45 Ferrando C, Suarez-Sipmann F, Mellado-Artigas R, Hernández M, Gea A, Arruti E *et al.* Clinical features, ventilatory management, and outcome of ARDS caused by COVID-19 are similar to other causes of ARDS. *Intens Care Med* 2020; **46**: 2200–2211.
- 46 Gattinoni L, Coppola S, Cressoni M, Busana M, Rossi S, Chiumello D. Covid-19 Does Not Lead to a “Typical” Acute Respiratory Distress Syndrome. *Am J Resp Crit Care* 2020; **0**: 1299–1300.
- 47 Carissimo G, Xu W, Kwok I, Abdad MY, Chan Y-H, Fong S-W *et al.* Whole blood immunophenotyping uncovers immature neutrophil-to-VD2 T-cell ratio as an early marker for severe COVID-19. *Nat Commun* 2020; **11**: 5243.
- 48 Farina A, Peruzzi G, Lacconi V, Lenna S, Quarta S, Rosato E *et al.* Epstein-Barr virus lytic infection promotes activation of Toll-like receptor 8 innate immune response in systemic sclerosis monocytes. *Arthritis Res Ther* 2017; **19**: 39.
- 49 Rempel H, Calosing C, Sun B, Pulliam L. Sialoadhesin expressed on IFN-induced monocytes binds HIV-1 and enhances infectivity. *PLoS ONE* 2008; **3**: e1967.
- 50 Carvelli J, Demaria O, Vély F, Batista L, Benmansour NC, Fares J *et al.* Association of COVID-19 inflammation with activation of the C5a–C5aR1 axis. *Nature* 2020; **588**: 146–150.
- 51 Liao M, Liu Y, Yuan J, Wen Y, Xu G, Zhao J *et al.* Single-cell landscape of bronchoalveolar immune cells in patients with COVID-19. *Nature medicine* 2020; **26**: 842–844.

- 52 Bastard P, Rosen LB, Zhang Q, Michailidis E, Hoffmann H-H, Zhang Y *et al.* Autoantibodies against type I IFNs in patients with life-threatening COVID-19. *Science* 2020; **370**: eabd4585.
- 53 Zhang Q, Bastard P, Liu Z, Pen JL, Moncada-Velez M, Chen J *et al.* Inborn errors of type I IFN immunity in patients with life-threatening COVID-19. *Science* 2020; **370**: eabd4570.
- 54 Galbraith MD, Kinning KT, Sullivan KD, Baxter R, Araya P, Jordan KR *et al.* Seroconversion stages COVID19 into distinct pathophysiological states. *Elife* 2021; **10**: e65508.
- 55 Stolk RF, Pasch E van der, Naumann F, Schouwstra J, Bressers S, Herwaarden AE van *et al.* Norepinephrine Dysregulates the Immune Response and Compromises Host Defense during Sepsis. *Am J Resp Crit Care* 2020; **202**: 830–842.
- 56 Reyes M, Filbin MR, Bhattacharyya RP, Sonny A, Mehta A, Billman K *et al.* Induction of a regulatory myeloid program in bacterial sepsis and severe COVID-19. *Biorxiv* 2020; : 2020.09.02.280180.
- 57 Thompson EA, Cascino K, Ordonez AA, Zhou W, Vaghasia A, Hamacher-Brady A *et al.* Mitochondrial induced T cell apoptosis and aberrant myeloid metabolic programs define distinct immune cell subsets during acute and recovered SARS-CoV-2 infection. *Medrxiv Prepr Serv Heal Sci* 2020. doi:10.1101/2020.09.10.20186064.
- 58 Xu G, Qi F, Li H, Yang Q, Wang H, Wang X *et al.* The differential immune responses to COVID-19 in peripheral and lung revealed by single-cell RNA sequencing. *Cell Discov* 2020; **6**: 73.
- 59 Sánchez-Cerrillo I, Landete P, Aldave B, Sánchez-Alonso S, Sánchez-Azofra A, Marcos-Jiménez A *et al.* COVID-19 severity associates with pulmonary redistribution of CD1c+ DC and inflammatory transitional and nonclassical monocytes. *J Clin Invest* 2020; **130**: 6290–6300.
- 60 Fan E, Beitler JR, Brochard L, Calfee CS, Ferguson ND, Slutsky AS *et al.* COVID-19-associated acute respiratory distress syndrome: is a different approach to management warranted? *Lancet Respir Medicine* 2020; **8**: 816–821.
- 61 Levey AS, Eckardt K-U, Tsukamoto Y, Levin A, Coresh J, Rossert J *et al.* Definition and classification of chronic kidney disease: A position statement from Kidney Disease: Improving Global Outcomes (KDIGO). *Kidney Int* 2005; **67**: 2089–2100.
- 62 Ponikowski P, Voors AA, Anker SD, Bueno H, Cleland JGF, Coats AJS *et al.* 2016 ESC Guidelines for the diagnosis and treatment of acute and chronic heart failureThe Task Force for the diagnosis and treatment of acute and chronic heart failure of the European Society of Cardiology (ESC)Developed with the special contribution of the Heart Failure Association (HFA) of the ESC. *Eur Heart J* 2016; **37**: 2129–2200.
- 63 Gall JRL. A new Simplified Acute Physiology Score (SAPS II) based on a European/North American multicenter study. *Jama J Am Medical Assoc* 1993; **270**: 2957–2963.

64 Gaudriot B, Uhel F, Gregoire M, Gacouin A, Biedermann S, Roisne A *et al.* Immune Dysfunction After Cardiac Surgery with Cardiopulmonary Bypass. *Shock* 2015; **44**: 228–233.

65 Balci PL, Pinceaux K, Pronier C, Seguin P, Tadié J-M, Reizine F. Herpes simplex virus and cytomegalovirus reactivations among severe COVID-19 patients. *Crit Care* 2020; **24**: 530.

Journal Pre-proof

Highlights

- Machine-learning analysis of CyTOF data segregates Covid-19⁺ and Covid-19⁻ ARDS
- CD169⁺S100A9⁺ monocytes differentiate Covid-19 ARDS from other ARDS
- Monocyte compartment alterations correlate with other immune subset modifications
- CD14⁺HLA-DR^{lo} and CD14^{lo}CD16⁺ monocytes are markers of adverse Covid-19 evolution

eTOC Blurb

Roussel et al. characterize the immune profile of COVID-19⁺ and COVID-19⁻ patients, both presenting an acute respiratory distress syndrome (ARDS) and COVID-19⁺ without ARDS. They identify a COVID-19 signature associating CD169⁺S100A9⁺ monocytes, plasmablasts, and Th1 cells. CD14⁺HLA-DR^{lo} and CD14^{lo}CD16⁺ monocytes increase during the ICU stay correlate with unfavorable clinical course.

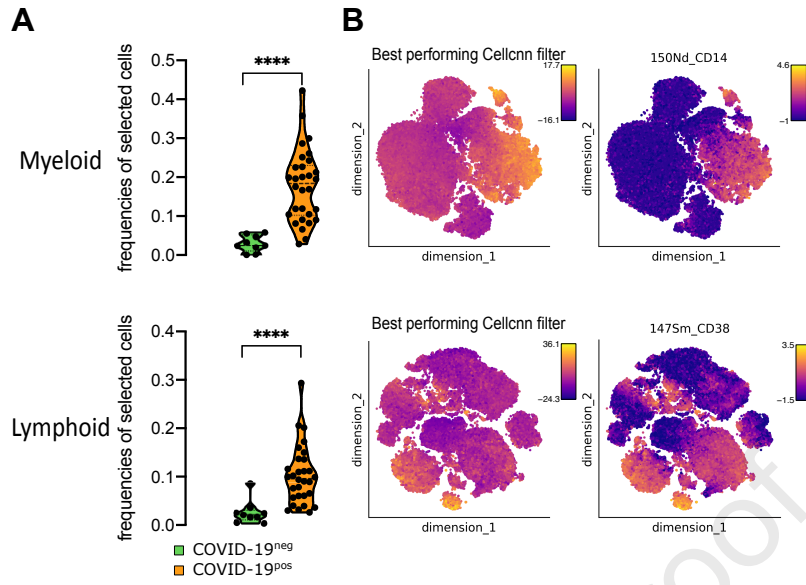


Figure 1

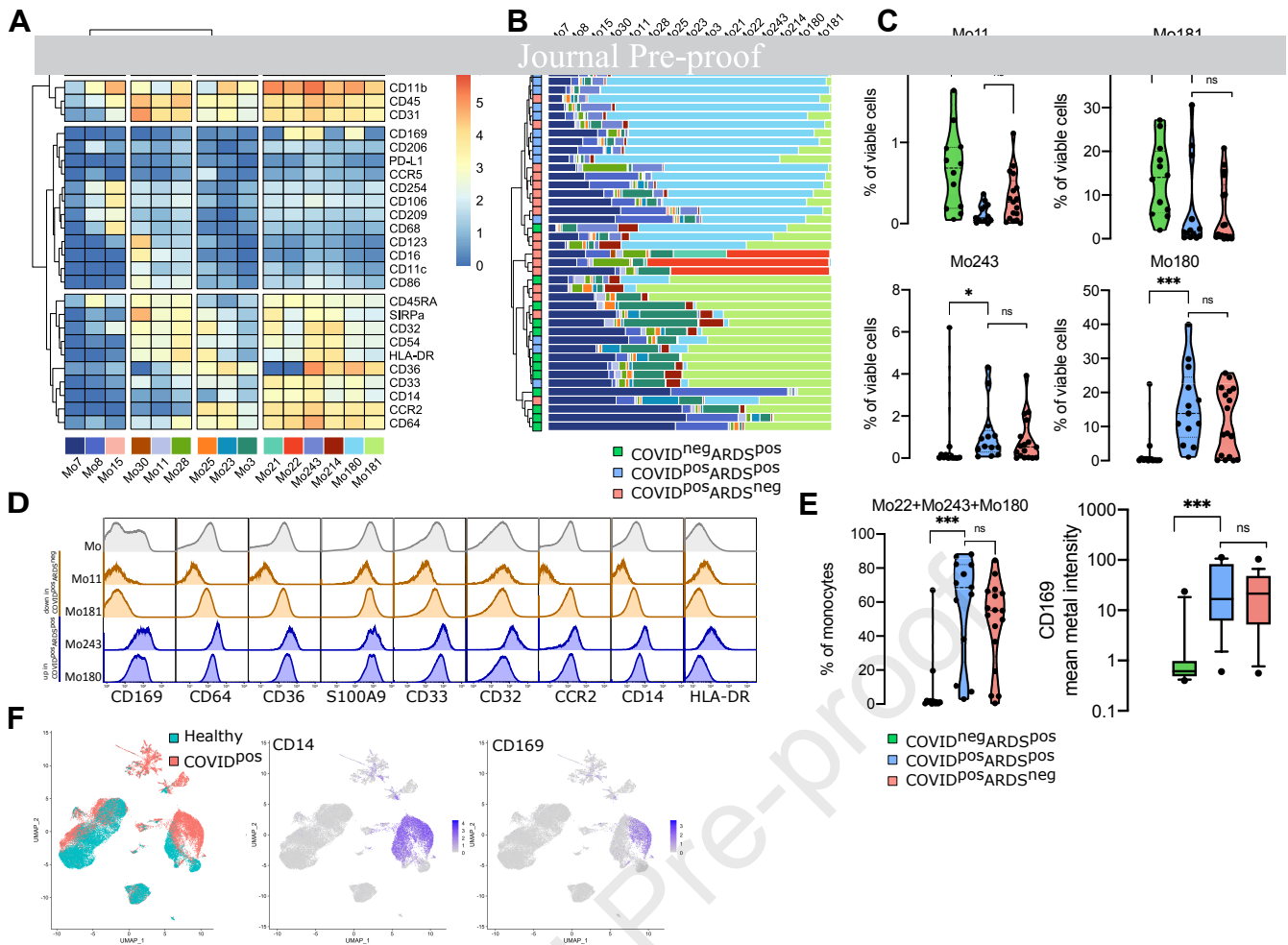


Figure 2

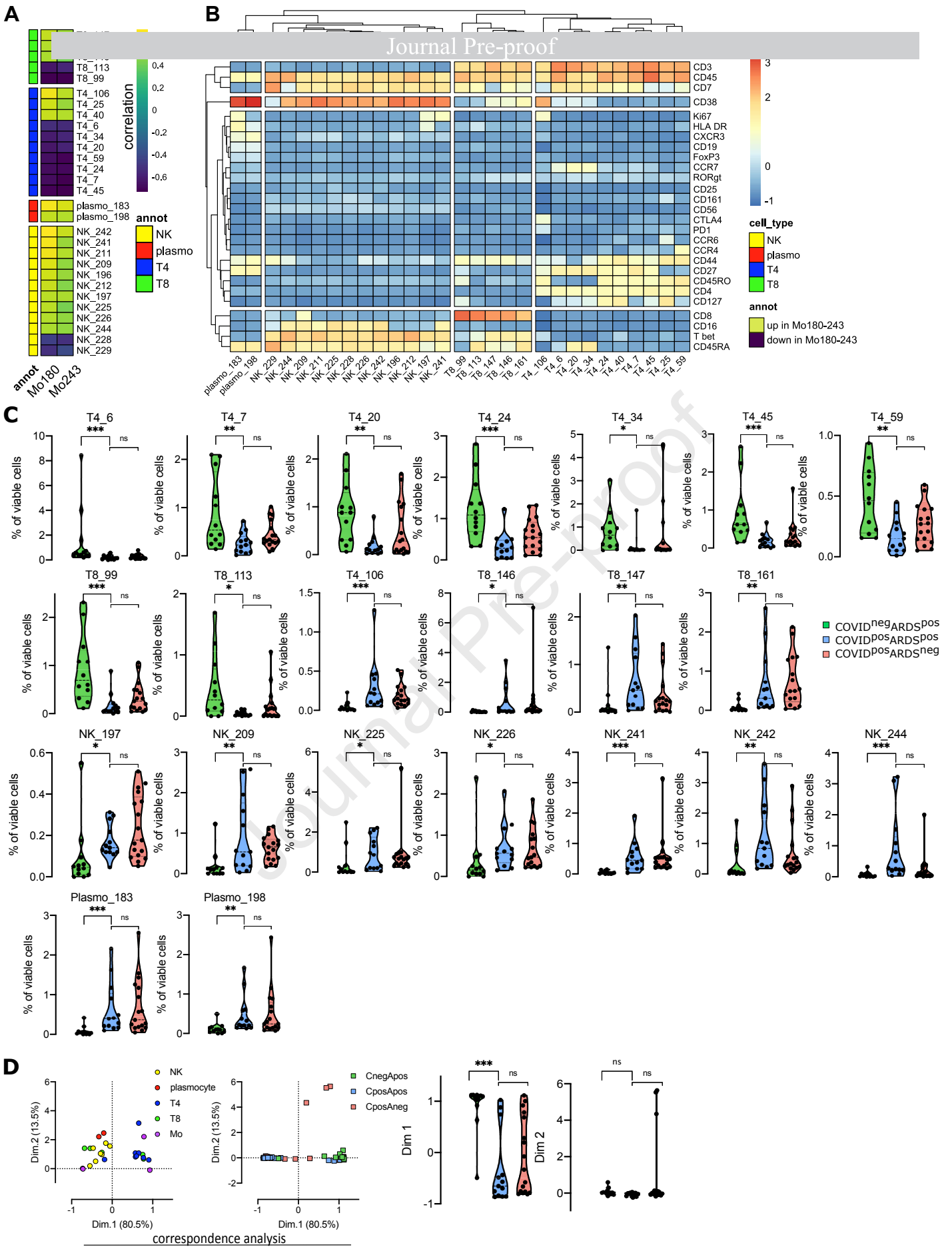


Figure 3

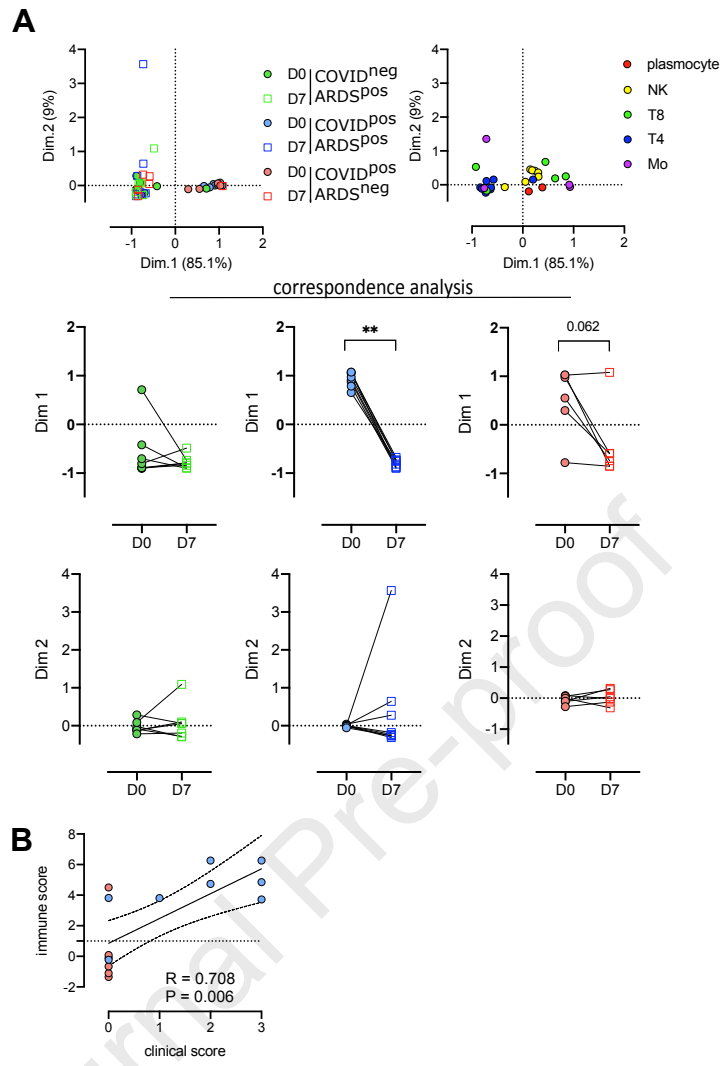


Figure 4